


# Force Display Control System using 2 DOF Admittance Control in Surgical Training Simulator with Chiseling Operation

Kentaro Masuyama<sup>1</sup>, Yoshiyuki Noda<sup>2</sup><sup>a</sup>, Yasumi Ito<sup>2</sup>, Yoshiyuki Kagiya<sup>2</sup> and Koichiro Ueki<sup>3</sup>

<sup>1</sup>*Integrated Graduate School of Medicine, Engineering and Agricultural Sciences, University of Yamanashi, Kofu, Yamanashi, Japan*

<sup>2</sup>*Faculty of Engineering Department, University of Yamanashi, Kofu, Yamanashi, Japan*

<sup>3</sup>*Faculty of Medicine, University of Yamanashi, Chuo, Yamanashi, Japan*

**Keywords:** Surgical Training Simulator, Virtual Reality, Force Display Device, Chiseling, 2 DOF Admittance Control.

**Abstract:** This study contributes to developing the virtual surgical training simulator for chiseling operation. In surgical operations using the bone chisel, impact forces are applied to the bone by pounding the chisel with the mallet. To virtually represent this situation in the training simulator, the force display system with high stiffness and instant reaction to the impact force is needed. In order to realize this force display system, we constructed the force display device with the ball-screw mechanism for obtaining the high stiffness, and proposed the two degree-of-freedom (2 DOF) admittance control for reacting instantaneously in the previous study. In this study, the force display control system using 2 DOF admittance control is analyzed, and the feedforward and feedback controllers in 2 DOF admittance control are developed for improving the reaction of the force display device. The efficacy of the proposed control system is verified by creating a virtual experience to the chiseling manipulation of a hard object using the bone mallet. From the experimental results, it is confirmed that the movement, contact, chiseling and splitting sensations are displayed more accurately than the conventional approach.

## 1 INTRODUCTION


Surgical training simulators with force display have been recently developed to allow surgeons to get into their surgical skills. The simulated environment allows vision, hearing and force sensory immersion so that trainees can practice surgical procedures repeatedly and safely with high realistic sensation (Maier et al., 2019), (Lam et al., 2013). In recent studies, devices with force display have used either the parallel mechanism, which the end effector is connected directly with three independent links (Hung et al., 2018), or the serial link mechanism, which the links are joined serially from the base to the end effector (Bugdadi et al., 2018). These devices with force display make possible to exhibit the high degree-of-freedom (DOF) of motion and high response, which allows creating high realistic sensation for surgical training with soft tissues.

However, in oral and orthopedic surgeries, large forces are applied to the bone and tooth as hard tissues by using the drill, saw and chisel. Previously proposed force display devices can be broken by ap-

plying the necessary large impact forces used in the surgeries to the hard tissues, and be limited to input of small force (Yanping et al., 2014), (Wijewickrema et al., 2018). Especially, virtualizing the situation that the surgeon chisels the hard tissue by pounding with the mallet requires the force display device with high stiffness for withstanding the impact force and high response for reacting instantaneously to the impact force.

In the previous study by the present authors (Masuyama et al., 2018), the force display device with the ball-screw mechanism was constructed for having high stiffness, and the 2 DOF admittance control was proposed for reacting instantaneously to the impact force. However, the feedforward and feedback controllers in the 2 DOF admittance control for creating high realistic sensation have not been designed reasonably in the previous study.

In this study, we propose the design of force display control system using the 2 DOF admittance control for creating high realistic sensation to the chisel operation. The 2 DOF admittance control for force display is analyzed theoretically. Then, the feedforward and the feedback controllers in the 2 DOF admittance control are designed in accordance with the

<sup>a</sup> <https://orcid.org/0000-0001-8500-5529>

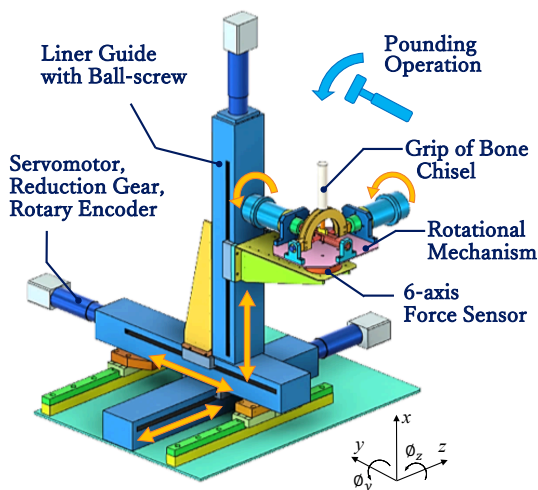


Figure 1: Force Display Device for Surgical Training Simulator Using Bone Chisel.

analysis. The efficacy of the proposed force display control system is verified by the experiments of virtual chiseling operation using the force display with high stiffness.

## 2 FORCE DISPLAY DEVICE

An illustration of the proposed force display device for the virtual surgical simulator with chiseling the hard tissue is shown in Fig. 1. This device has 5 DOF motion, which the chisel can move to  $x$ -,  $y$ - and  $z$ -directions and rotate to  $\phi_y$ - and  $\phi_z$ -directions. The translational motion of the force display device is realized using a ball-screw mechanism to have the high stiffness so that it withstands the impact force by pounding the mallet. The mass of the moving object on  $y$ -axis is 17[kg]. The maximum display force on the translational motion is 100[N] and the maximum display torque on the rotational motion is 7.5[Nm], respectively. The maximum velocity on the translational motion is 0.76[m/s] and the maximum angular velocity on the rotational motion is 1181[deg/s], respectively. The maximum transfer distance of the chisel in each direction is 0.29[m]. Both maximum rotational angles of the chisel in  $\phi_y$ - and  $\phi_z$ -directions are same as 65[deg]. These specifications of the force display device satisfy to create the realistic surgical simulation using the chisel.

The 6-axis force sensor is installed at the base of the chisel's rotational mechanism. The impact or manipulation force added to the chisel can be measured by the force sensor.

## 3 ANALYSIS OF FORCE DISPLAY CONTROL SYSTEM

In the analysis of the force display control system, the 2 DOF admittance control is compared with a general admittance control. The force display control system is required that the motion of the drive system precisely reproduces the output from the virtual model. Therefore, the transfer characteristics of both the general and the 2 DOF admittance controls are discussed as follows.

### 3.1 Admittance Control

The general admittance control installed to a single axis is shown in Fig. 2, where  $F$  is the operational force measured by the force sensor,  $F_v$  is the modified operational force through the low-pass filter,  $u$  is the input command,  $x_d$  is the position of the tip of the chisel,  $d$  is the disturbance,  $P_D$  is the dynamics of the drive system,  $P_V$  is the virtual model that represents the chiseling operation of the hard tissue by pounding the chisel with the mallet, and  $L_F$  is the low-pass filter used for suppressing the sensor noise. Generally, this admittance control scheme has been used for constructing the force display device.

It is necessary to analyze the responsiveness of the admittance control as shown in Fig. 2. The system-wide transfer function is represented as

$$X_d(s) = P_D(s)P_V(s)L_F(s)F(s) + P_D(s)D(s), \quad (1)$$

where  $s$  is a Laplace operator. Thus, the responsiveness of the force display device can be degraded by the response lags of the drive system,  $P_D$ , and the low-pass filter,  $L_F$ . Moreover, it is difficult to reproduce precisely the response of the virtual model, when the disturbances occur in the drive system.

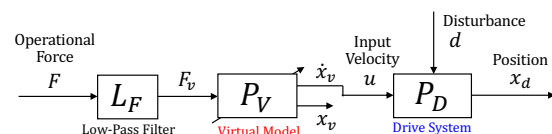


Figure 2: Block Diagram of Admittance Control.

### 3.2 2 DOF Admittance Control

The block diagram of the 2 DOF admittance control proposed by the present authors(Masuyama et al., 2018) is shown in Fig. 3. The system-wide transfer

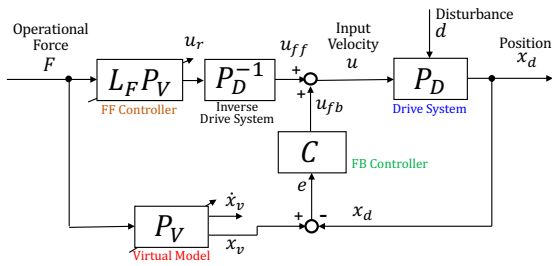


Figure 3: Block Diagram of 2 DOF Admittance Control.

function can be represented as

$$X_d(s) = \frac{P_V(s)(L_F(s) + P_D(s)C(s))}{1 + P_D(s)C(s)} F(s) + \frac{P_D(s)}{1 + P_D(s)C(s)} D(s), \quad (2)$$

where  $C$  is the feedback controller. The gain characteristics of the low-pass filter in the frequency domain is represented as

$$|L_F(\omega)| = \left| \frac{X_d(\omega)}{F(\omega)} \right| = \frac{1}{\sqrt{\omega^2/\omega_f^2 + 1}}, \quad (3)$$

where  $\omega$  is the angular frequency, and  $\omega_f$  is the cut-off angular frequency. Therefore, the gain of the low-pass filter in the low-frequency range converges as  $L_F \rightarrow 1$ , and the transfer function  $X_d/F$  can be represented as

$$\left. \frac{X_d(s)}{F(s)} \right|_{\omega \rightarrow 0} = \frac{P_V(s)(1 + P_D(s)C(s))}{1 + P_D(s)C(s)} = P_V(s). \quad (4)$$

The dynamics of the drive system and the low-pass filter can be ignored in the low-frequency range.

However, the gain of the low-pass filter in the high-frequency range converges as  $L_F \rightarrow 0$ . The gain of the transfer function  $X_d/F$  in the high-frequency range can be represented as

$$\left. \frac{X_d(s)}{F(s)} \right|_{\omega \rightarrow \infty} = \frac{P_V(s)P_D(s)C(s)}{1 + P_D(s)C(s)}. \quad (5)$$

Then, increasing the gain of the feedback controller as  $P_D(s)C(s) \gg 1$  allows the responsiveness of the force display device to be improved as

$$\left. \frac{X_d(s)}{F(s)} \right|_{P_D(s)C(s) \gg 1} = P_V(s). \quad (6)$$

The ideal responsiveness in the high-frequency range can be realized by the feedback controller with high gain. Moreover, the disturbance can also be suppressed by increasing the gain of the feedback controller  $C(s)$  as

$$\left. \frac{X_d(s)}{D(s)} \right|_{P_D(s)C(s) \gg 1} = \frac{1}{C(s)} \approx 0. \quad (7)$$

Therefore, the responsiveness and disturbance suppression of the control system in the force display device can be improved by the 2 DOF admittance control with high gain feedback controller as mentioned above.

The mathematical representations of each block are described in the following sections.

#### 4 DRIVE SYSTEM MODEL: $P_D$

The servomotors are applied to the drive system on each axis as shown in Fig. 1, and the velocity feedback control is implemented in each servomotor system. Therefore, the drive system can be represented as

$$\ddot{x}_d(t) = -\frac{1}{T_m} \dot{x}_d(t) + \frac{K_m}{T_m} u(t), \quad (8)$$

where  $T_m$  is the time constant in seconds, and  $K_m$  is the gain. The time constants and the gains are identified as  $T_{mx}=4.93[\text{ms}]$  and  $K_{mx}=1.00$  in x-direction,  $T_{my}=4.91[\text{ms}]$  and  $K_{my}=1.00$  in y-direction, and  $T_{mz}=5.76[\text{ms}]$  and  $K_{mz}=1.00$  in z-direction, respectively.

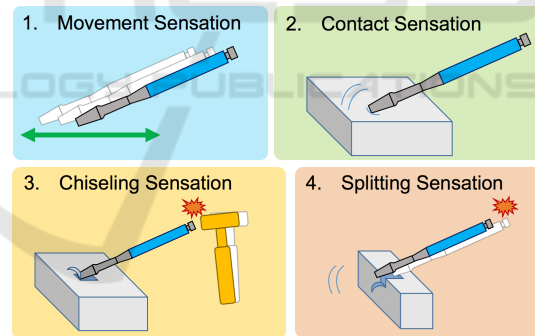


Figure 4: Situations between Chisel and Hard Tissue.

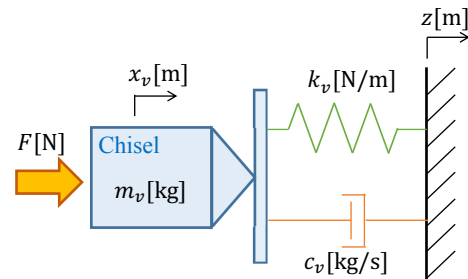


Figure 5: Dynamics of Virtual Model.

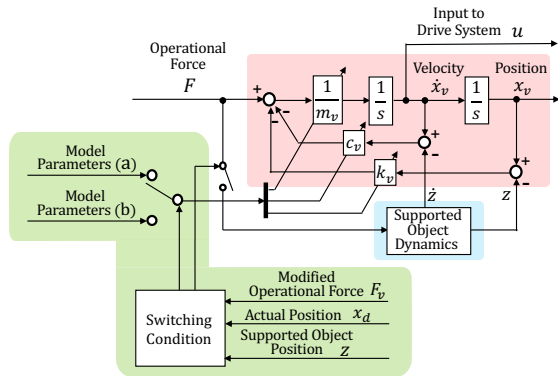


Figure 6: Block Diagram of Virtual Model.

## 5 VIRTUAL MODEL OF CHISELING OPERATION: $P_V$

The virtual model is the source of the force representation for creating the operating sensation of the chisel, which is illustrated in Fig. 4. These situations can be represented in the virtual model shown in Fig. 5. The dynamics of the virtual model is represented as

$$m_v \ddot{x}_v(t) + c_v(\dot{x}_v(t) - \dot{z}(t)) + k_v(x_v(t) - z(t)) = F(t), \quad (9)$$

where  $x_v$  is the position of the tip of chisel in the virtual model and  $z$  is the position of the supported object. The model parameters  $m_v$ ,  $k_v$ , and  $c_v$  are the mass, spring constant and viscosity coefficient in the virtual model represented as a spring-mass-damper system, respectively. The hard contact sensation can be created by the virtual model with high viscoelastic characteristics. The chiseling sensation by pounding with the mallet is created by the movement of the supported object.

### 5.1 Derivation of Parameters in Virtual Model

The block diagram of the virtual model is shown in Fig. 6. The model parameters  $m_v$ ,  $k_v$ , and  $c_v$  can be varied in accordance with the situations. In the situation that the chisel is contacting to the hard tissue, the model parameters can be derived by transforming the virtual model of Eq. (9) to the generalized form as

$$\ddot{x}_v + 2\zeta\omega_n\dot{x}_v + \omega_n^2x_v = 2\zeta\omega_n\dot{z} + \omega_n^2z + K\omega_n^2F, \quad (10)$$

where

$$\omega_n = \sqrt{\frac{k_v}{m_v}}, \quad \zeta = \frac{c_v}{2\sqrt{m_vk_v}}, \quad K = \frac{1}{k_v}. \quad (11)$$

Table 1: Parameters of Virtual Model on Situations.

	Situation	Model Parameters		
		$m_v$ [kg]	$c_v$ [kg/s]	$k_v$ [N/m]
(a)	Contacting Hard Tissue	100	$1.2 \times 10^4$	$3.6 \times 10^5$
(b)	Chisel in Air	2	20	0

	Generalized Parameters			
	$\omega_n$ [rad/s]	$\zeta$	$\omega_c$ [rad/s]	$K$
(a)	60	1	-	$2.8 \times 10^{-6}$
(b)	-	-	10	$5.0 \times 10^{-2}$

$\omega_n$  is the natural angular frequency,  $\zeta$  is the damping ratio and  $K$  is the gain of the virtual model. In the situation that the chisel is manipulated in the air, since the spring element and the supported object are removed from the virtual model, the virtual model can be transformed to the first order-lag system with the integrator as

$$\ddot{x}_v + \omega_c \dot{x}_v = K\omega_c F, \quad (12)$$

where

$$\omega_c = \frac{c_v}{m_v}, \quad K = \frac{1}{c_v}. \quad (13)$$

$\omega_c$  is the cut-off angular frequency. We adjust the model parameters based on the generalized forms represented in Eqs. (10), (12).

The model parameters for each situation are shown in Table 1. The damping ratio  $\zeta$  in the situation (a) is given as  $\zeta=1$  for suppressing the vibration. The other parameters in the situation (a) can be obtained experimentally such that they are increased until the chisel stays against the operational force. On the other hand, the parameters in the situation (b) can be obtained such that they are decreased until the chisel can be moved freely.

The contact sensation on the hard tissue is created by switching the model parameters from (b) to (a). The split sensation is created by switching the model parameters from (a) to (b). The switching condition of the model parameters is shown as

$$[m_v, c_v, k_v] = \begin{cases} \text{Model Parameters (a),} \\ (F_v > 0 \wedge z \leq x_d \leq \delta \wedge 0 \leq z \leq \delta), \\ \text{Model Parameters (b), (else),} \end{cases} \quad (14)$$

where  $\delta$  is the width of the hard tissue,  $F_v$  is the modified operational force through the low-pass filter,  $L_F$ . In this study, the width of the hard object is  $\delta=10$ [mm], the supported object position is firstly  $z=0$ [m].



### 5.2 Movement of Supported Object

The movement of the supported object should be designed based on the actual chiseling operation. The relation between the pounding force with the mallet and the travel distance of tip of the chisel can be measured in the actual chiseling operation. In this study, the acrylic plate is used as the chiseled object for facilitating to obtain the hard tissue and be able to measure easily the travel distance of tip of the chisel. The acrylic plate used in this experiment is shown in Fig. 7, and the chisel and the mallet are shown in Fig. 8. The experimental environment of the actual chiseling operation with the acrylic plate is illustrated as Fig. 9. To measure the pounding force with the mallet, the acrylic plate and the force detector are clamped with the vices. The chisel angle is fixed to 30[deg] by the fixture placed under the chisel. The tip travel distance of the chisel is exactly measured with the slide caliper.

The experimental results of the relation between the pounding forces and the tip travel distance of the chisel are shown as Fig. 10. The circle and the plus markers are shown as the tip travel distances caused by weak and strong pounding forces, respectively. These relations are modeled by the least squares method and represented as

$$\Delta z(F) = 6.38 * 10^{-5} F(t) - 3.81 * 10^{-4}. \quad (15)$$

The supported object position is shown as

$$z = \sum \Delta z(F), \quad (z \leq x_d \wedge 0 \leq z \leq \delta \wedge F \geq F_d), \quad (16)$$

where  $F_d$  is the dead band of the pounding force with mallet. In this study, the force dead band is  $F_d=30[N]$ .

### 6 LOW-PASS FILTER: $L_F$

The low-pass filter is applied in front of the virtual model to reduce sensor noise and represented as

$$\dot{F}_v = -\omega_f F_v + \omega_f F. \quad (17)$$

The cut-off angular frequency used for the purposes of this study is  $\omega_f=10[\text{rad/s}]$ .  $\omega_f$  can be determined by the preliminary experiments. In the experiment,  $\omega_f$  is increased until the vibrating motion is caused. And, the largest frequency is selected in the condition with suppressing the vibration.

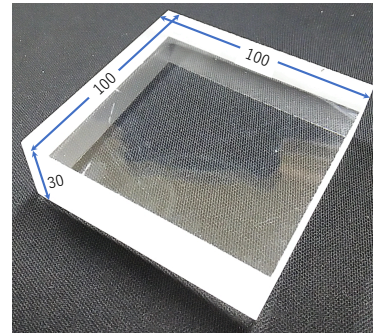


Figure 7: Acrylic Plate.

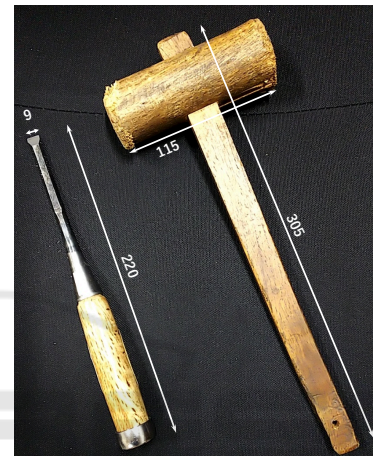


Figure 8: Chisel and Mallet.

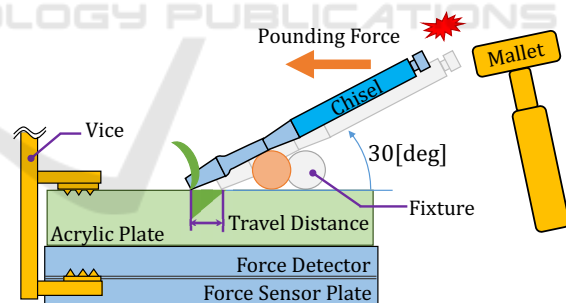


Figure 9: Illustration of Actual Chiseling Operation with Acrylic Plate.

### 7 DESIGN OF FEEDBACK CONTROLLER: $C$

A phase lead compensator is applied to the feedback controller for increasing the gain in the high-frequency range. The phase lead compensator can be represented as

$$C(s) = k \frac{1 + \alpha T s}{1 + T s}, \quad (k, T > 0, \alpha > 1), \quad (18)$$

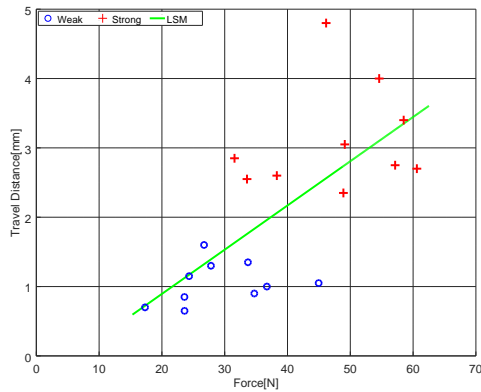


Figure 10: Experimental Results of Chiseling Operation with Acrylic Plate.

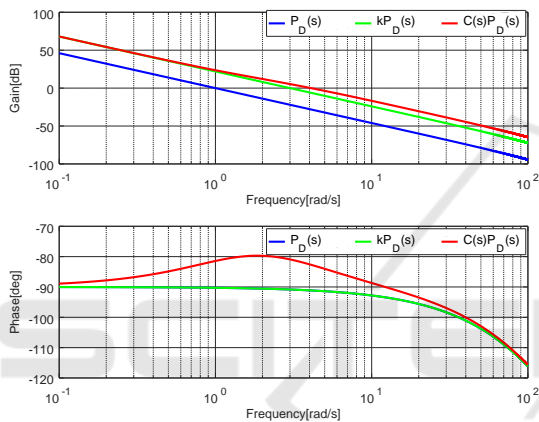


Figure 11: Bode Diagram of Open Loop Systems with/without Compensator.

where  $k$  is the gain,  $\alpha$  and  $T$  are the control parameters in this compensator. These parameters are designed such that the controller gain in the high-frequency range is risen, while the vibration is suppressed. In this study, the gain is  $k=3$ , the parameters in the controller are  $\alpha=1.46$  and  $T=0.42$ . The frequency characteristics of this phase lead compensator is shown as Fig. 11. The frequency band of the high-frequency range can be improved by this phase lead compensator.

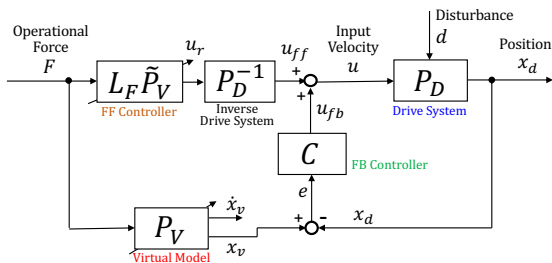


Figure 12: Block Diagram of 2 DOF Admittance Control.

## 8 DESIGN OF FEEDFORWARD CONTROLLER: $L_F P_V$

The feedforward controller consists of the low-pass filter and the virtual model. The contact sensation can be degraded by the difference of the responses between the feedforward controller,  $L_F P_V$ , and the proper virtual model,  $P_V$ . Thus, the virtual model in the feedforward controller is modified as  $L_F \tilde{P}_V$ . The modified virtual model  $\tilde{P}_V$  can be derived as

$$m_v \ddot{x}_v(t) + c_v \dot{x}_v(t) - \dot{z}(t) = F_v(t), \quad (19)$$

By the modification of the virtual model in the feedforward controller,  $\tilde{P}_V$ , the contact sensation in accordance with the proper virtual model may not be represented precisely. Therefore, we analyze the 2 DOF admittance control system with the modified virtual model in the feedforward controller as below.

The system-wide transfer function of the 2 DOF admittance control which is modified the virtual model to Eq.(19) can be represented as

$$\begin{aligned} \frac{X_d(s)}{F(s)} &= \frac{\tilde{P}_V(s)L_F(s) + P_V(s)P_D(s)C(s)}{1 + P_D(s)C(s)} \\ &= \frac{(1 + \frac{k_v}{m_v s^2 + c_v s})L_F(s) + P_D(s)C(s)}{1 + P_D(s)C(s)} P_V(s). \end{aligned} \quad (20)$$

The gain of the low-pass filter in the high-frequency range decreases as  $L_F \rightarrow 0$  and can be shown as

$$\begin{aligned} \left. \frac{X_d(s)}{F(s)} \right|_{\substack{P_D(s)C(s) \gg 1 \\ \omega \rightarrow \infty}} &= \frac{P_D(s)C(s)}{1 + P_D(s)C(s)} P_V(s) \\ &= P_V(s). \end{aligned} \quad (21)$$

Thus, the proper virtual model  $P_V$  can be represented in the high-frequency range.

However, the gain of the low-pass filter in the low-frequency range converges as  $L_F \rightarrow 1$  and can be shown as

$$\left. \frac{X_d(s)}{F(s)} \right|_{\omega \rightarrow 0} = \frac{\frac{k_v}{m_v s^2 + c_v s} + 1 + P_D(s)C(s)}{1 + P_D(s)C(s)} P_V(s). \quad (22)$$

Here, the operation in the low-frequency range is in the movement sensation as shown in Fig. 4. The virtual spring constant in the movement sensation is  $k_v=0$ [N/m] as shown in Table 1. Therefore, the gain of the transfer function  $X_d/F$  in low-frequency range can be shown as

$$\left. \frac{X_d(s)}{F(s)} \right|_{\omega \rightarrow 0} = \frac{1 + P_D(s)C(s)}{1 + P_D(s)C(s)} P_V(s) = P_V(s). \quad (23)$$

Thus, even if the virtual model is modified as Eq.(19), the virtual model can be reproduced properly by the proposed 2 DOF admittance control.

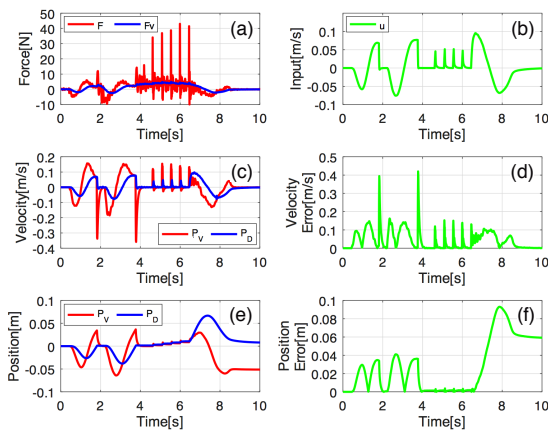


Figure 13: Experimental Results by Using Conventional Admittance Control.

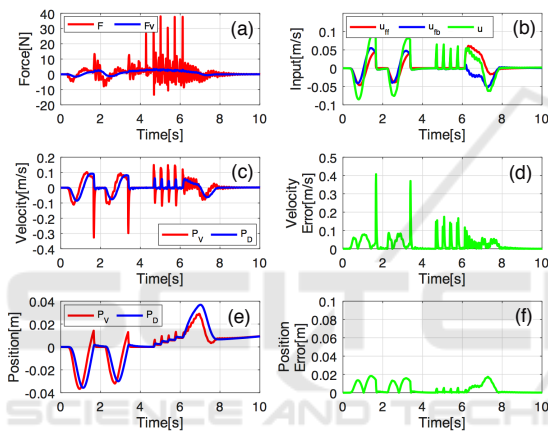


Figure 14: Experimental Results by Using 2 DOF Admittance Control.

## 9 EXPERIMENTAL RESULTS

The efficacy of the proposed 2 DOF admittance control is verified by comparing with the conventional admittance control. In order to confirm that the representation of the proper virtual model can be created precisely by the proposed approach, we evaluate the error between the outputs of the proper virtual model and the drive system.

The experimental results using the conventional admittance control are shown in Fig. 13, where (a) shows the operational force measured by the force sensor, (b) is the input command to the drive system, (c) and (e) are the velocity and the position of the tip of chisel and, (d) and (f) are the absolute error of the velocity and the position, respectively. We show only the motion on the  $y$ -axis due to space limitations. We also obtain similar results on the other axes. The edge of the hard tissue is located at  $x_d=0$ [mm]. The transla-

tional motion of the chisel is stopped at  $x_d=0$ [mm], as seen around 2[s] and 4[s]. As seen from these results, the sensation caused by contacting the hard tissue can be created. There are some impact forces arisen by pounding the chisel with the mallet after 4[s]. The tip of chisel is moved instantaneously with moving the supported object. After the impulse of the impact forces reached to the width of the hard object, 10[mm], the split sensation has created.

On the other hand, the experimental results using the 2 DOF admittance control are shown in Fig. 14. The graphs in Fig. 14 are same arrangement to Fig. 13. The errors of the velocity and the position in the movement, chiseling and splitting operation are smaller using the proposed 2 DOF admittance control than the conventional one. Therefore, the sensation to operate the chisel is created precisely by implementing the proposed 2 DOF admittance control.

## 10 CONCLUSION

A force display device with high stiffness and 2 DOF admittance control system that can instantaneously react to impact forces were proposed for the simulations of surgical procedures using a bone chisel. The experimental results showed that the absolute errors of the velocity and the position can be decreased by the proposed 2 DOF admittance control.

In the future, it is required to develop the virtual model which represents adequately the chiseling sensation to the hard tissue for realizing the surgical simulator with high realistic sensation.

## REFERENCES

- Bugdadi, A., Sawaya, R., Bajunaid, K., Olwi, D., Winkler-Schwartz, A., Ledwos, N., Marwa, I., Alsaidiri, G., Sabbagh, A. J., Alotaibi, F. E., Al-Zhrani, G., and Maestro, R. D. (2018). Is virtual reality surgical performance influenced by force feedback device utilized? In *Journal of Surgical Education*. Vol.76, pp.262-273.
- Hung, V., Mihai, V., Dragana, C., Ion, I., and Paraschiv, N. (2018). Dynamic computation of haptic-robot devices for control of a surgical training system. In *International Journal of Computing*. Vol.17, No.2, pp.81-93.
- Lam, C., Sundaraj, K., and Sulaiman, M. N. (2013). Virtual reality simulator for phacoemulsification cataract surgery education and training. In *Procedia Computer Science*. Vol.18, pp.742-748.
- Maier, J., Weiherer, M., Huber, M., and Palm, C. (2019). Imitating human soft tissue on basis of a dual-material 3d print using a support-filled metamaterial to provide bimanual haptic for a hand surgery training system. In

*Quantitative Imaging in Medicine and Surgery*. Vol.9, No.1, pp.30-42.

- Masuyama, K., Noda, Y., Ito, Y. and Kagiya, Y., and Ueki, K. (2018). Force display device and control system for surgical training simulator using bone chisel. In *IEEE International Conference on Biomedical Robotics and Biomechatronics*. pp.1248-1253.
- Wijewickrema, S., Copson, B., Ma, X., Briggs, R., Bailey, J., Kennedy, G., and O'Leary, S. (2018). Development and validation of a virtual reality tutor to teach clinically oriented surgical anatomy of the ear. In *IEEE International Symposium on Computer-Based Medical Systems*. pp.12-17.
- Yanping, L., Xudong, W., Fule, W., Xiaojun, C., Chengtao, W., and Guofang, S. (2014). Development and validation of a surgical training simulator with haptic feedback for learning bone-sawing skill. In *Journal of Biomedical Informatics*. Vol.48, pp.122-129.

